

Equation of state and phase diagram of FeO

Rebecca A. Fischer^{a,*1}, Andrew J. Campbell^{a,1}, Gregory A. Shofner^a, Oliver T. Lord^{b,2},
Przemyslaw Dera^c, and Vitali B. Prakapenka^c

^aDepartment of Geology, University of Maryland, College Park, MD 20742, USA

^bDepartment of Earth Sciences, University of Bristol, Wills Memorial Building, Queen's
Road, Bristol, BS81RJ, UK

^cCenter for Advanced Radiation Sources, 9700 South Cass Avenue, Building 434A,
Argonne, IL 60439, USA

*Corresponding author. Email: rfischer@uchicago.edu. Phone: (773) 834-1085. Fax:
(773) 702-9505

¹Present address: Department of the Geophysical Sciences, University of Chicago, 5734
South Ellis Avenue, Chicago, Illinois 60637, USA

²Present address: Department of Earth Sciences, University College London, Gower
Street, London, WC1E 6BT, UK

Submitted to *Earth and Planetary Science Letters* October 4, 2010

Revised February 9, 2011

Accepted February 14, 2011

Abstract

Wüstite, Fe_{1-x}O , is an important component in the mineralogy of Earth's lower mantle and may also be a component in the core. Therefore the high pressure, high temperature behavior of FeO, including its phase diagram and equation of state, is essential knowledge for understanding the properties and evolution of Earth's deep interior. We performed X-ray diffraction measurements using a laser-heated diamond anvil cell to achieve simultaneous high pressures and temperatures. Wüstite was mixed with iron metal, which served as our pressure standard, under the assumption that negligible oxygen dissolved into the iron. Our data show a positive slope for the subsolidus phase boundary between the B1 and B8 structures, indicating that the B1 phase is stable at the P - T conditions of the lower mantle and core. We have determined the thermal equation of state of B1 FeO to 156 GPa and 3100 K, finding an isothermal bulk modulus $K_0 = 149.4 \pm 1.0$ GPa and its pressure derivative $K_0' = 3.60 \pm 0.4$. This implies that 7.7 ± 1.1 weight percent oxygen is required in the outer core to match the seismologically-determined density, under the simplifying assumption of a purely Fe-O outer core.

Keywords: wüstite; high pressure; equations of state; phase equilibria; oxygen fugacity

1. Introduction

Wüstite, Fe_{1-x}O , is an important endmember of $(\text{Mg,Fe})\text{O}$ in the Earth's lower mantle and possibly also a significant alloying component of the core (McDonough, 2003). Iron is the most abundant multivalent element in the mantle; its oxidation state dominates the redox chemistry of the mantle, in turn controlling element partitioning, phase equilibria, diffusion, and related physical and chemical properties (Frost and McCammon, 2008). If oxygen is a primary light element component in the core, then its impact on the density of Fe-rich melts is critical to interpreting the composition, dynamics, and evolution of the core. Therefore it is essential to understand the high pressure, high temperature phase relations and thermodynamics of the Fe-O system. In this study we focus on the thermal equation of state and subsolidus phase diagram of stoichiometric iron oxide, FeO.

Under ambient conditions wüstite is stable in the B1 (NaCl-type) crystal structure. With room temperature compression it undergoes a rhombohedral $\bar{R}\bar{3}$ (Mao et al., 1996) distortion around 17 GPa, with the transition pressure depending on the degree of hydrostaticity (Fei, 1996; Fei and Mao, 1994). This distortion has also been reported to be a monoclinic $C2/m$ phase, both at high pressures (Kantor et al., 2008) and at 1 bar and low temperatures (Fjellvåg et al., 2002). Diamond cell and shock wave experiments show a transformation of wüstite to the B8 (NiAs-type) crystal structure at high pressures and temperatures (Fei and Mao, 1994; Jeanloz and Ahrens, 1980; Knittle and Jeanloz, 1991; Kondo et al., 2004; Murakami et al., 2004; Ozawa et al., 2010; Yagi et al., 1988), based

on X-ray diffraction and electrical resistivity measurements. However, the location and slope of the B1/B8 transition is inconsistent among these studies, with some reporting a vertical slope around 70 GPa at high temperatures (Knittle and Jeanloz, 1991; Murakami et al., 2004; Yagi et al., 1988) and others indicating a strongly positive slope in pressure-temperature space (Kondo et al., 2004; Ozawa et al., 2010). Some investigators have failed to observe the transition to the B8 phase altogether (Mao et al., 1996; Sata et al., 2005; Seagle et al., 2008; Yagi et al., 1985), and have attributed this to differences in stoichiometry (Seagle et al., 2008) or kinetic barriers at room temperature (Mao et al., 1996). The melting curve of Fe_{1-x}O has been determined up to pressures and temperatures of 77 GPa and 3100 K (Fischer and Campbell, 2010), with reasonable agreement between multi-anvil press (Ringwood and Hibberson, 1990) and diamond anvil cell experiments (Boehler, 1992; Fischer and Campbell, 2010; Shen et al., 1993).

The thermal equation of state of FeO is important for interpreting the seismological structure of the Earth's lower mantle and the density deficit, relative to pure iron, of Earth's outer core. Room temperature studies have shown that the degree of nonstoichiometry in wüstite does not significantly affect its bulk modulus (Fei, 1996), although some ambiguity remains (Mao et al., 1996; McCammon, 1993). The equation of state and high pressure phase transition in wüstite has also been studied by shock compression (Jeanloz and Ahrens, 1980; Yagi et al., 1988). A recent static compression study expanded the equation of state of FeO to high temperatures, where the B1 (non-distorted) phase is stable to much higher pressure (Campbell et al., 2009); this yielded an isothermal bulk modulus $K_0 = 146.9$ GPa with a fixed pressure derivative $K_0' = 4$.

In this study, we aim to constrain the B1/B8 phase boundary of FeO using X-ray diffraction in a laser-heated diamond anvil cell, to resolve between existing discrepancies in the literature data. We also aim to determine the thermal equation of state of B1 FeO at higher pressures and temperatures than previous studies (Campbell et al., 2009), extending the existing dataset into the P - T region of the outer core. This will allow for calculations of the amount of oxygen required to match the observed density deficit in the outer core, and also improved understanding of the iron-iron oxide oxygen fugacity buffer at core conditions, with minimal extrapolation required over pressure and temperature.

2. Experimental Methods

The equation of state of FeO was determined by measuring its lattice parameter using synchrotron X-ray diffraction during laser-heating in a diamond anvil cell. The FeO was mixed with metallic Fe to ensure that the oxide was saturated in iron, and presumably stoichiometric, at high pressures and temperatures (Campbell et al., 2009; Seagle et al., 2008; Stølen and Grønvold, 1996). Seagle et al. (2008) laser heated wüstite +Fe mixtures up to 93 GPa and found the recovered samples to be stoichiometric; we assume a similar equilibration took place in our higher pressure sample, but this could not be verified directly because the anvils broke before decompression and the sample was destroyed.

Sample material was prepared by mixing $\text{Fe}_{0.94}\text{O}$ powder ($a = 4.302 \pm 0.001 \text{ \AA}$; McCammon and Liu, 1984) with Fe powder in a ratio of 1:1.23 by mass, which produces a ~10 wt% oxygen content in the mixture. The mixture was mechanically ground under ethanol to a grain size of ~1 μm , then dried in an oven at 85°C for one hour. The powder was pressed in a diamond anvil cell to form a foil approximately 70 μm in diameter and 5 μm thick. A rhenium gasket, initially 250 μm thick, was preindented to ~27 GPa, and a hole 80 μm in diameter in the center of the indentation served as the sample chamber. Beveled diamond anvils were used, with 150 μm flats and an 8° bevel out to 300 μm . The sample was loaded between two layers of NaCl ~10 μm thick, which acted as the pressure medium and thermal insulator. The sample assembly was oven-dried at 85°C for one hour after cell loading but before pressurization.

Angle-dispersive X-ray diffraction experiments were performed at beamline 13-ID-D (GeoSoilEnviroCars) of the Advanced Photon Source, Argonne National Laboratory (Prakapenka et al., 2008; Shen et al., 2005). The incident X-ray beam was monochromatic ($\lambda = 0.3344 \text{ \AA}$) and measured 5 μm x 5 μm . Diffracted X-rays were recorded using a MAR165 CCD detector, with the sample-to-detector distance calibrated by 1 bar diffraction of CeO_2 . Exposure times were typically 5 s.

The X-ray diffraction patterns were integrated to produce two-theta plots using Fit2D (Hammersley et al. 2006). Peak fitting of the integrated patterns was performed using PeakFit (Systat Software). Overlapping peaks were deconvoluted in nearly all cases. Overlapped peaks that could not be deconvoluted were not used, except in a small number of cases when necessary to constrain the uncertainty for a hexagonal phase, and

when their use or exclusion did not change the calculated lattice parameter within error. Pressures were determined from the volume of hcp-iron, using the thermal equation of state of Dewaele et al. (2006). This equation of state was calibrated against both room temperature and shock wave compression to >200 GPa, and includes an explicit, theoretically derived electronic contribution. Uncertainties in pressure were calculated based on the uncertainty in temperature and the uncertainty in the lattice parameters of hcp-iron, which were determined from four to seven d-spacings. The NaCl pressure medium acted as a secondary pressure standard (Fei et al., 2007).

Our calculation of pressure is based on the unit cell volume of iron and the temperature of the sample, corrected for an axial temperature gradient (Campbell et al., 2007). In using iron as the pressure standard, we are assuming both mechanical and thermal equilibrium between the Fe and FeO, which were intimately mixed (Campbell et al., 2009). Deviatoric stresses on the sample are expected to be negligible, as are compositional inhomogeneities that might place the pressure standard and the sample material under slightly different P - T conditions. We are also assuming that there is no dissolved oxygen in the iron that is altering its unit cell volume, which is supported by an earlier study of recovered Fe+FeO samples (Ozawa et al., 2010).

The sample was compressed to a target pressure and laser-heated from each side by 1.064 μm Yb fiber lasers with ‘flat top’ profiles created by Pi-shaping optics, with the laser power on each side being independently adjustable (Prakapenka et al., 2008). The temperature was slowly stepped up by increasing the laser power until a target temperature was reached, and then the laser power was decreased gradually to zero, with

diffraction patterns being obtained both on heating and cooling cycles. Temperatures were determined spectroradiometrically (Heinz and Jeanloz, 1987) using the graybody approximation over the 600-800 nm range of thermal emission, and were measured during the collection of each diffraction pattern. The laser-heated spots were $\sim 20\text{-}25\ \mu\text{m}$ in diameter, much larger than the X-ray beam to minimize radial temperature gradients, and were coaligned with the beam using X-ray induced fluorescence from the NaCl insulator. Upstream and downstream laser powers were adjusted during heating to equalize the intensity of the thermal emission on the two surfaces of the sample. All temperature measurements used in this study were recorded on the upstream side of the sample, because of technical difficulties with measurements on the downstream side during this set of experiments. Temperatures were measured from a region $5\ \mu\text{m}$ in diameter in the center of the laser-heated spot, comparable in size to the area probed by the X-rays.

Temperatures measured on the surface of the sample were corrected downward by 3% to account for an axial temperature gradient through the thickness of the sample, based on a sample thickness of $\sim 5\ \mu\text{m}$ (Campbell et al., 2007, 2009). Reported uncertainties in temperature incorporate an analytical uncertainty of 100 K (Shen et al., 2001), as well as the uncertainty from the correction for the axial temperature gradient (Campbell et al., 2007, 2009).

To verify the accuracy of the temperature measurements, a sample of pure iron loaded in an MgO pressure medium was analyzed to check the location of the hcp-fcc phase transition in iron. The sample was pressurized to $36.4 \pm 0.5\ \text{GPa}$ before heating,

based on the lattice parameter of hcp-Fe (Dewaele et al., 2006). The phase transition in iron was bracketed between volumes and temperatures of $6.014 \pm 0.006 \text{ cm}^3/\text{mol}$, $1563 \pm 107 \text{ K}$ (hcp-Fe) and $6.140 \pm 0.080 \text{ cm}^3/\text{mol}$, $1609 \pm 108 \text{ K}$ (fcc-Fe) on heating, which agrees with the published phase diagram of Komabayashi and Fei (2010).

3. Results

The pressure-volume-temperature (P - V - T) data from the synchrotron X-ray diffraction experiments are listed in Table S1 of the Supplementary Material. The lattice parameters of hcp-Fe were calculated from four to seven of the following peaks: 100, 002, 101, 102, 110, 103, 112. The lattice parameter of B1-FeO was determined from three to six of the following peaks: 111, 200, 220, 311, 222, 400, 331, and those of B8-FeO were calculated from up to four of the following peaks: 002, 100, 101, 102, 112, 104, 202. A unit cell volume for B8-FeO is only reported when at least two non-overlapping peaks were observed. In addition, the lattice parameter of B2-NaCl was determined from the observed d -spacings of three to six of the following hkl peaks: 100, 110, 111, 200, 211, 220. Figure 1a and b shows a diffraction pattern collected at 144 GPa and 3025 K with peaks corresponding to B2-NaCl, B1-FeO, and hcp-Fe, while Figure 1c shows a pattern collected at 151 GPa and 1665 K with peaks corresponding to B2-NaCl, B8-FeO, and hcp-Fe.

Figure 2 illustrates the comparison of our B1-FeO P - V - T data with those of Seagle et al. (2008), Campbell et al. (2009), and Ozawa et al. (2010), which were all synchrotron X-ray diffraction studies of wüstite coexisting with metallic iron. All of these data were obtained using a laser-heated diamond anvil cell, except for the data up to ~ 10 GPa from Campbell et al. (2009), which were obtained in a multi-anvil press. This study and Ozawa et al. (2010) report pressures based on the unit cell volume of hcp-Fe (Dewaele et al., 2006); for comparison, the pressures of the Seagle et al. (2008) and Campbell et al. (2009) data have been recalculated based on the unit cell volume of iron, using the equation of state of hcp-Fe (Dewaele et al., 2006) or fcc-Fe (Campbell et al., 2009). These studies had originally reported pressures based on the unit cell volume of B1- or B2-NaCl; the difference in calculated pressure between the NaCl and Fe pressure standards for those data is 0.3%, on average.

Figure 3 shows our B8-FeO P - V - T data and those of Ozawa et al. (2010). Also shown for comparison are the lone data point from Kondo et al. (2004), who studied Fe_{0.95}O using ruby fluorescence to measure the pressure (Mao et al., 1978), and the lone data point from Fei and Mao (1994), who studied Fe_{0.98}O and used the equation of state of gold (Anderson et al., 1989) to calculate the pressure.

Figure 4 shows the phase diagram of FeO. The B1 and B8 phases of FeO were frequently seen to coexist in these experiments. Presumably this is hysteresis from the kinetics of the transformation, as well as a contribution from the aforementioned thermal gradients in the laser-heated sample. We determined the phase boundary by monitoring the growth in relative intensities of several peaks in each phase. For example, P - T

conditions in which the B1 peak intensities were increasing and the B8 peak intensities were decreasing relative to the previous X-ray diffraction pattern were assigned to the B1 stability field (Kondo et al., 2004; Murakami et al., 2010).

4. Discussion

4.1. B1/B8 phase transition

The B1/B8 phase boundary observed in this study is broadly consistent with that of Kondo et al. (2004), but at slightly lower temperatures than would be expected from the results of Ozawa et al. (2010) (Figure 4). The disagreement between these datasets could be due to the large uncertainties in temperature reported by Ozawa et al. (2010); otherwise, the high degree of curvature required for a phase boundary to match both of those datasets, in addition to the present results, is unlikely. Our data are incompatible with the phase boundaries of Fei and Mao (1994), but it is important to note that we measured the B1/B8 transition, while they measured the rhombohedral/B8 transition, at temperatures far from the triple point. However, any B1/B8/rhombohedral triple point based on our data and those of Fei and Mao (1994) would be in violation of Schreinemaker's rules (Zen, 1966), because of the angles between the phase boundaries at the B1/B8/rhombohedral triple point that are required by the combination of our data with those of Fei and Mao (1994) (Figure 4). One or more additional phase boundaries

could also resolve these apparent disagreements in the phase diagram of wüstite, but no such transitions were detected in this study.

Our B1/B8 transition matches the shock wave results of Jeanloz and Ahrens (1980) within the large uncertainty of their temperature measurement, but it is inconsistent with the high-pressure phase transition reported by Knittle and Jeanloz (1991). Knittle and Jeanloz (1991) did not obtain any structural information, so their results could correspond to an electronic transition that is distinct from the B1/B8 transition.

Regardless of these small inconsistencies between various studies, our phase diagram confirms the conclusion of Ozawa et al. (2010) that it is the B1 structure of FeO, not the B8 structure, that is stable under the P - T conditions relevant to the Earth's lower mantle and outer core. Therefore, it is the equation of state of B1-FeO that we apply to calculations of the core density deficit and oxygen fugacity buffers (Sections 4.3 and 4.4).

4.2. Equations of state

Our new higher-pressure P - V - T data on B1-FeO are not precisely described by an extrapolation of the equation of state of Campbell et al. (2009), with the extrapolated equation of state predicting pressures in excess of 5 GPa higher than those measured. Therefore, we have redetermined the equation of state of B1-FeO, expanding the dataset used by Campbell et al. (2009) with the addition of higher P - T data from this study and from Ozawa et al. (2010), which allows us to fit more parameters in the equation of state.

We have also constructed an equation of state for B8-FeO, which had not previously been determined for iron-saturated wüstite.

We fit P - V - T datasets of B1- and B8-FeO to Mie-Grüneisen equations of state,

$$P = P_{300}(V) + (\gamma/V)[E(\theta_D, T) - E_{300}(\theta_D, 300)] \quad (1)$$

with the 300 K isothermal pressure (P_{300}) described by a third-order Birch-Murnaghan equation of state (Birch, 1952) and the thermal pressure term based on a Debye model of vibrational energy (E), with Grüneisen parameter $\gamma = \gamma_0(V/V_0)^q$ and Debye temperature $\theta_D = \theta_0 * \exp[\gamma_0/q*(1 - (V/V_0)^q)]$. We did not explicitly include any anharmonic or electronic contributions to the thermal pressure. This reduced the number of fitted parameters, which was necessary given the resolution of our data.

The equation of state parameters for B1- and B8-FeO are listed in Table 1. For B1-FeO, we fit the present data along with those of several previous studies (Campbell et al., 2009; Ozawa et al., 2010; Seagle et al., 2008). We fixed the parameters V_0 (McCammon and Liu, 1984), θ_0 (Stixrude and Lithgow-Bertelloni, 2007), and q , finding a good fit to the data for $q = 0.5$. Our fitted values of K_0 and K_0' (149.4 GPa and 3.60, respectively) show excellent agreement with the trade-off for these parameters determined by Fei (1996) for B1-FeO, whose preferred values were 149 GPa and 3.5. Isotherms calculated from our equation of state of B1-FeO are shown in Figure 2. We find that K_0' must be less than four to fit the higher-pressure data, which explains the misfit between these data and the extrapolated equation of state of Campbell et al. (2009), who fixed K_0' to 4.0 in their analysis.

For B8-FeO, we fit the present data along with those of Ozawa et al. (2010). This phase is not recoverable to ambient conditions, so V_0 is a fitted parameter, and a reduction in the number of other fitted parameters was achieved by fixing $K_0' = 4$ and $q = 1$ and assuming the Debye temperature to be equal to that of B1-FeO (Stixrude and Lithgow-Bertelloni, 2007). It was necessary to hold these parameters fixed due to the limited P - T range of the B8 data, and as a consequence, this equation of state should not be extrapolated far outside the range of the data. The zero-pressure volume V_0 for B8-FeO was found to be 2.1% smaller than that of B1-FeO (McCammon and Liu, 1984) (Table 1). We found a lower value of K_0 for B8-FeO than for B1-FeO (137.8 GPa vs. 149.4 GPa), but we used a higher value of K_0' for the B8 phase, so it is less compressible at the high pressure conditions under which it exists. We also found different values of γ_0 for the two phases, but their γ become very similar at high pressures due to the different q values in the fits. Isotherms calculated from our equation of state of B8-FeO are shown in Figure 3. There is significant misfit between our equation of state and the data points of Fei and Mao (1994) and Kondo et al. (2004). Both of these studies used non-stoichiometric wüstite, while this study and Ozawa et al. (2010) used iron-saturated FeO, but stoichiometric effects should cause the data of Fei and Mao (1994) and Kondo et al. (2004) to be shifted to smaller volumes of wüstite, whereas their data have larger volumes than are predicted by our equation of state (Figure 3). The cause of this discrepancy is unknown, though it could have the same underlying basis as the disagreement over the B1/B8 phase boundary between our data and those of Fei and Mao (1994) (Section 4.1). The data point of Kondo et al. (2004) does agree with our equation

of state within its large pressure uncertainty, but the misfit should be greater taking into account the effects of stoichiometry.

4.3. Core density deficit

We can use the knowledge that wüstite is stable in the B1 structure under the P - T conditions of the Earth's core (Section 4.1) and our improved equation of state for B1-FeO at core conditions (Section 4.2) to evaluate the core density deficit. Several assumptions are required for this analysis. We assume the pressure at the core-mantle boundary (CMB) to be 135.8 GPa (Dziewonski and Anderson, 1981), and we use an outer core temperature of 4000 ± 500 K at the CMB based on the analysis of Anderson (2003). We also assume that the outer core is convecting near adiabatic conditions (Birch, 1952), and that iron and iron-rich alloys experience a 1-2% volume increase upon melting at core pressures (Anderson, 2003). Although it is likely that the outer core contains significant amounts of more than one light element, including O, S, Si, and/or C (McDonough, 2003), in this analysis we consider an outer core whose light element component is purely oxygen.

Figure 5 illustrates the density difference between pure iron (Dewaele et al., 2006), calculated along an adiabat, and a seismologically-determined density profile of the Earth's core, the Preliminary Reference Earth Model (PREM) (Dziewonski and Anderson, 1981). Using the assumptions described above, we find that PREM is $10.4 \pm 0.9\%$ less dense than solid hcp-iron at the core-mantle boundary. Approximately 1-2% of this density difference can be accounted for by the ΔV of melting of iron (Anderson,

2003), but the remainder must be due to the presence of one or more light elements in the core, such as oxygen.

Our equation of state for B1-FeO can be used to place firm constraints on the amount of oxygen in Earth's core, because it requires no extrapolation in pressure and only a small extrapolation in temperature to be applied at the P - T conditions of the CMB. For a core model containing only iron and oxygen, we find that 7.7 ± 1.1 weight percent oxygen would be required in the outer core to match PREM at the core-mantle boundary. Allowing for the presence of nickel in the core slightly alters this result. Correcting the outer core density to account for a Ni/Fe atomic ratio of 0.058 in the core (McDonough, 2003), we find that 7.9 ± 1.1 weight percent oxygen would be necessary to match PREM at the CMB for an Fe-Ni-O core.

Figure 5 shows that the slopes of the adiabatic density profiles of hcp-Fe and B1-FeO do not exactly match that of PREM when these equations of state are extrapolated over the P - T range of the Earth's core. Their slopes also do not match each other, due to the K_0' value for FeO being smaller than that of iron (3.60 vs. 5.38) (Dewaele et al., 2006). For this reason, we have limited our calculations of the core density deficit to the core-mantle boundary, minimizing extrapolation. If oxygen is the dominant light element in the core, these differences in curvature could be due to several factors, including: PREM not accurately describing the precise density variations through the core; the need for an additional term in these equations of state when extrapolating them to such high pressures and temperatures; a compositional gradient through the outer core; a more

complex mixing relationship between Fe and FeO at these conditions; or the presence of one or more other light elements.

4.4. Oxygen fugacity buffer

Oxygen fugacity (fO_2) governs many key physical and chemical properties of minerals, including insulator-metal transitions, diffusion rates, rheological properties, and elemental partitioning. The fO_2 of the Earth's interior is dominated by the valence state of iron, the most abundant multivalent element in the planet. Therefore it is critical to understand the Fe-FeO oxygen fugacity buffer at pressures and temperatures relevant to the deep Earth. In this study we have extended the equation of state of B1-FeO to higher P - T conditions, allowing us to extend calculations of the Fe-FeO fO_2 buffer to these more extreme conditions.

We have calculated this buffer by comparing the equations of state of B1-FeO (Section 4.2), fcc-Fe (Campbell et al., 2009), and hcp-Fe (Dewaele et al., 2006), following the method of Campbell et al. (2009):

$$\log fO_2 = \log fO_2(1\text{bar}) + (0.8686/RT) \int \Delta V dP \quad (2)$$

where ΔV is the volume difference between FeO and iron. The calculated buffer is strictly applicable only for FeO in the B1 structure, and only for high-spin FeO. Iron-poor (Mg,Fe)O in the Earth's lower mantle may undergo a spin transition to the low-spin state (Cohen et al., 1997; Lin et al., 2005), which will likely have a significant effect on the Fe-FeO oxygen fugacity buffer.

The calculated fO_2 buffers are shown in Figure 6, and tabulated values at smaller pressure increments are shown in Table S2 of the Supplementary Material. The results found here are similar to those presented in Campbell et al. (2009), with the buffers calculated in this study differing from those of Campbell et al. (2009) by less than 0.2 log units up to 100 GPa, the highest pressure shown by Campbell et al. (2009). However, this discrepancy increases with pressure, becoming larger at the higher pressures achieved in this study. We confirm the results of Campbell et al. (2009) that the absolute fO_2 values increase with pressure at each temperature, and that the slope $\partial(\ln fO_2)/\partial T|_P$ decreases with pressure, eventually becoming a slope of approximately zero at 60 GPa and negative at higher pressures. Also included in Table S2 is a polynomial expression of the Fe-FeO buffer as a function of pressure and temperature, which can be used as a convenience to interpolate between the tabulated values.

The oxygen fugacity buffers calculated in this section are specifically for stoichiometric FeO, because that is the endmember component in the important applications to high-pressure mineral physics and the chemistry of the Earth's mantle. In applications where FeO-bearing silicates or oxides exist with Fe-bearing metal, the oxygen fugacity of a system can be determined relative to the Fe-FeO buffer. Near ambient pressure, nonstoichiometric wüstite is the stable oxide that coexists with metallic iron, so the iron-wüstite buffer is frequently applied with respect to these nonstoichiometric oxides, especially when this solid state buffer is used directly to control the oxygen fugacity in low-pressure experiments. However, above several GPa, stoichiometric FeO becomes stable in the presence of Fe (Campbell et al., 2009; Seagle et

al., 2008; Stølen and Grønvold, 1996), so even when used directly to buffer a system, it is the Fe-FeO reaction that is relevant.

Nevertheless, it is interesting to consider whether nonstoichiometric wüstite becomes stable again at high pressures when coexisting with metallic Fe. The relevant reaction is $\text{Fe}_{1-x}\text{O} + x\text{Fe} \rightleftharpoons \text{FeO}$, and the pressure dependence of this reaction is determined by the volume difference $V(\text{FeO}) - V(\text{Fe}_{1-x}\text{O}) - xV(\text{Fe})$. The present study provides the equation of state of FeO, and equations of state exist for both fcc and hcp phases of Fe (e.g., Campbell et al., 2009; Dewaele et al., 2006), but the equations of state of wüstites are not precisely determined over the P - T range of interest. However, it has been concluded by Fei (1996) that the bulk modulus of Fe_{1-x}O is constant for all x ; if we suppose for purposes of this calculation that all other thermoelastic parameters are also independent of x , then we can evaluate the equation of state for any wüstite based on the equation of state parameters for FeO in this study (Table 1) and the zero-pressure lattice parameters of McCammon and Liu (1984). Our results of this calculation show that for all values of x , the volume change $V(\text{FeO}) - V(\text{Fe}_{1-x}\text{O}) - xV(\text{Fe})$ is negative over all conditions calculated (0 to 200 GPa; 300 to 2500 K). Therefore, stoichiometric FeO, and not nonstoichiometric wüstite, remains the stable oxide coexisting with Fe at all high P - T conditions above the several GPa range as reported by Stølen and Grønvold (1996).

5. Conclusions

The phase diagram of stoichiometric FeO, and the equations of state of its B1 and B8 structures, were measured to high temperatures and pressures reaching those of the Earth's outer core. The positive slope for the phase boundary between the subsolidus B1 and B8 phases of FeO is broadly consistent with those reported by Kondo et al. (2004) and Ozawa et al. (2010). These results confirm that the stable phase of FeO at conditions of the Earth's deep interior has the B1 structure, not the B8 structure. The equation of state of B1-FeO reported by Campbell et al. (2009) did not precisely describe these new higher pressure data, but the updated equation of state presented here accurately describes not only our new data but also those of several previous studies (Campbell et al., 2009; Ozawa et al., 2010; Seagle et al., 2008). We also combined our data with those of Ozawa et al. (2010) to construct an equation of state for B8-FeO.

Using our improved equation of state for B1-FeO and earlier equations of state for fcc- and hcp-Fe (Campbell et al., 2009; Dewaele et al., 2006), we have recalculated high-pressure, high-temperature Fe-FeO oxygen fugacity buffers, improving the accuracy of these buffers over those reported by Campbell et al. (2009) at pressures >100 GPa. The equation of state for B1-FeO can be compared to that of hcp-Fe (Dewaele et al., 2006) and the seismologically determined density of the Earth's core (Dziewonski and Anderson, 1981), to analyze the core density deficit. For a core composition in which oxygen is the sole light element, 7.9 ± 1.1 weight percent oxygen would be required in the outer core to match PREM at the core-mantle boundary.

Acknowledgments

Portions of this work were performed at GeoSoilEnviroCARS (Sector 13), Advanced Photon Source (APS), Argonne National Laboratory. GeoSoilEnviroCARS is supported by the National Science Foundation - Earth Sciences (EAR-0622171) and Department of Energy - Geosciences (DE-FG02-94ER14466). Use of the Advanced Photon Source was supported by the U. S. Department of Energy, Office of Science, Office of Basic Energy Sciences, under Contract No. DE-AC02-06CH11357. We thank the anonymous reviewers for constructive comments. This work was supported by the National Science Foundation by grant EAR 0847217 to A.J.C.

References

- Anderson, O.L., 2003. The three-dimensional phase diagram of iron, in: Dehant, V., Creager, K.C., Karato, S.-i., Zatman, S. (Eds.), *Earth's Core: Dynamics, Structure, Rotation*. American Geophysical Union, Washington, DC, pp. 83-103.
- Anderson, O.L., Isaak, D.G., Yamamoto, S., 1989. Anharmonicity and the equation of state for gold. *J. Appl. Phys.* 65, 1534-1543.
- Birch, F., 1952. Elasticity and constitution of the Earth's interior. *J. Geophys. Res.* 37, 227-286.
- Boehler, R., 1992. Melting of the Fe-FeO and the Fe-FeS systems at high pressure – constraints on core temperatures. *Earth Planet. Sci. Lett.* 111, 217-227.
- Boehler, R., 1996. Melting temperature of the Earth's mantle and core: Earth's thermal structure. *Annu. Rev. Earth Planet. Sci.* 24, 15-40.
- Campbell, A.J., Seagle, C.T., Heinz, D.L., Shen, G., Prakapenka, V.B., 2007. Partial melting in the iron-sulfur system at high pressure: A synchrotron X-ray diffraction study. *Phys. Earth Planet. Inter.* 162, 119-128.
- Campbell, A.J., Danielson, L., Richter, K., Seagle, C.T., Wang, Y., Prakapenka, V.B., 2009. High pressure effects on the iron-iron oxide and nickel-nickel oxide oxygen fugacity buffers. *Earth Planet. Sci. Lett.* 286, 556-564.
- Chase Jr., M.W., 1998. *NIST-JANAF Thermochemical Tables*, 4th ed. : J. Phys. Chem. Ref. Data Monograph No. 9. American Institute of Physics.

- Cohen, R.E., Mazin, I.I., Isaak, D.G., 1997. Magnetic collapse in transition metal oxides at high pressure: Implications for the Earth. *Science* 275, 654-657.
- Dewaele, A., Loubeyre, P., Occelli, F., Mezouar, M., Dorogokupets, P.I., Torrent, M., 2006. Quasihydrostatic equation of state of iron above 2 Mbar. *Phys. Rev. Lett.* 97, 215504.
- Dziewonski, A.M., Anderson, D.L., 1981. Preliminary reference Earth model. *Phys. Earth Planet. Inter.* 25, 297-356.
- Fei, Y., 1996. Crystal chemistry of FeO at high pressure and temperature, in: Dyar, M.D., McCammon, C., Schaefer, M.W. (Eds.), *Mineral Spectroscopy: A Tribute to Roger G. Burns*. The Geochemical Society, Houston, pp. 243-254.
- Fei, Y., Mao, H.-k., 1994. In-situ determination of the NiAs phase of FeO at high-pressure and temperature. *Science* 266, 1678-1680.
- Fei, Y., Ricolleau, A., Frank, M., Mibe, K., Shen, G., Prakapenka, V., 2007. Toward an internally consistent pressure scale. *Proc. Natl. Acad. Sci. U.S.A.* 104, 9182-9186.
- Fischer, R.A., Campbell, A.J., 2010. High pressure melting of wüstite. *Am. Mineral.* 95, 1473-1477.
- Fjellvåg, H., Hauback, B.C., Vogt, T., Stølen, S., 2002. Monoclinic nearly stoichiometric wüstite at low temperatures. *Am. Mineral.* 87, 347-349.
- Frost, D.J., McCammon, C.A., 2008. The redox state of Earth's mantle. *Annu. Rev. Earth Planet. Sci.* 36, 389-420.

- Hammersley, A.P., Svensson, S.O., Hanfland, M., Fitch, A.N., Hausermann, D., 1996. Two-dimensional detector software: From real detector to idealized image or two-theta scan. *High Press. Res.* 14, 235-248.
- Heinz, D.L., Jeanloz, R., 1987. Temperature measurements in the laser-heated diamond cell, in: Manghnani, M.H., Syono, Y. (Eds.), *High-Pressure Research in Mineral Physics*. Terra Scientific Publishing, Tokyo / American Geophysical Union, Washington, pp. 113-127.
- Jeanloz, R., Ahrens, T.J., 1980. Equations of state of FeO and CaO. *Geophys. J. R. astr. Soc.* 62, 505-528.
- Kantor, I., Kurnosov, A., McCammon, C., Dubrovinsky, L., 2008. Monoclinic FeO at high pressures. *Z. Krist.* 223, 461-464.
- Knittle, E., Jeanloz, R., 1991. The high-pressure phase diagram of Fe_{0.94}O: A possible constituent of the Earth's core. *J. Geophys. Res.* 96, 16169-16180.
- Komabayashi, T., Fei, Y., 2010. Internally consistent thermodynamic database for iron to the Earth's core conditions. *J. Geophys. Res.* 115, B03202.
- Kondo, T., Ohtani, E., Hirao, N., Yagi, T., Kikegawa, T., 2004. Phase transitions of (Mg,Fe)O at megabar pressures. *Phys. Earth Planet. Inter.* 143-144, 201-213.
- Lin, J.-F., Struzhkin, V.V., Jacobsen, S.D., Hu, M.Y., Chow, P., Kung, J., Liu, H., Mao, H.-k., Hemley, R.J., 2005. Spin transition of iron in magnesiowüstite in the Earth's lower mantle. *Nature* 436, 377-380.

- Mao, H.-k., Bell, P.M., Shaner, J.W., Steinberg, D.J., 1978. Specific volume measurements of Cu, Mo, Pd, and Ag and calibration of the ruby R₁ fluorescence pressure gauge from 0.06 to 1 Mbar. *J. Appl. Phys.* 49, 3276-3283.
- Mao, H.-k., Shu, J., Fei, Y., Hu, J., Hemley, R.J., 1996. The wüstite enigma. *Phys. Earth Planet. Inter.* 96, 135-145.
- McCammon, C., 1993. Effect of pressure on the composition of the lower mantle end member Fe_xO. *Science* 259, 66-68.
- McCammon, C.A., Liu, L.-G., 1984. The effects of pressure and temperature on non-stoichiometric wüstite, Fe_xO: The iron-rich phase boundary. *Phys. Chem. Miner.* 10, 106-113.
- McDonough, W.F., 2003. Compositional model for the Earth's core, in: Carlson, R.W. (Ed.), *Treatise of Geochemistry*, Vol. 2. Elsevier-Pergamon, Oxford, pp. 547-568.
- Murakami, M., Hirose, K., Ono, S., Tsuchiya, T., Isshiki, M., Watanuki, T., 2004. High pressure and high temperature phase transitions of FeO. *Phys. Earth Planet. Inter.* 146, 273-282.
- Ozawa, H., Hirose, K., Tateno, S., Sata, N., Ohishi, Y., 2010. Phase transition boundary between B1 and B8 structures of FeO up to 210 GPa. *Phys. Earth Planet. Inter.* 179, 157-163.
- Prakapenka, V.B., Kuba, A., Kuznetsov, A., Laskin, A., Shkurikhin, O., Dera, P., Rivers, M.L., Sutton, S.R., 2008. Advanced flat top laser heating system for high pressure research at GSECARS: Application to the melting behavior of germanium. *High Press. Res.* 28, 225-235.

- Ringwood, A.E., Hibberson, W., 1990. The system Fe-FeO revisited. *Phys. Chem. Miner.* 17, 313-319.
- Sata, N., Hirose, K., Oshino, Y., Shen, G., 2005. High-pressure experiments on FeO up to 200 GPa. *EOS Trans. AGU 86, Fall Meet. Suppl.*, Abstract MR31A-0124.
- Seagle, C.T., Heinz, D.L., Campbell, A.J., Prakapenka, V.B., Wanless, S.T., 2008. Melting and thermal expansion in the Fe-FeO system at high pressure. *Earth Planet. Sci. Lett.* 265, 655-665.
- Shen, G., Lazor, P., Saxena, S.K., 1993. Melting of wüstite and iron up to pressures of 600 kbar. *Phys. Chem. Minerals* 20, 91-96.
- Shen, G., Mao, H.-K., Hemley, R.J., Duffy, T.S., Rivers, M.L., 1998. Melting and crystal structure of iron at high pressures. *Geophys. Res. Lett.* 25, 373–376.
- Shen, G.Y., River, M.L., Wang, Y.B., Sutton, S.R., 2001. Laser heated diamond anvil cell system at the Advanced Photon Source for in situ x-ray measurements at high pressure and temperature. *Rev. Sci. Instrum.* 72, 1273-1282.
- Shen, G., Rivers, M.L., Wang, Y., Sutton, S.R., 2005. Facilities for high-pressure research with the diamond anvil cell at GSECARS. *J. Synchrotron Rad.* 12, 642-649.
- Stixrude, L., Lithgow-Bertelloni, C., 2007. Influence of phase transformations on lateral heterogeneity and dynamics in Earth's mantle. *Earth Planet. Sci. Lett.* 263, 45-55.
- Stølen, S., Grønvold, F., 1996. Calculation of the phase boundaries of wüstite at high pressure. *J. Geophys. Res.* 101, 11531–11540.
- Yagi, T., Suzuki, K., Akimoto, S., 1985. Static compression of wüstite (Fe_{0.98}O) to 120 GPa. *J. Geophys. Res.* 90, 8784-8788.

Yagi, T., Fukuoka, K., Takei, H., Syono, Y., 1988. Shock compression of wüstite.

Geophys. Res. Lett. 15, 816-819.

Zen, E.-A., 1966. Construction and pressure-temperature diagrams for multicomponent systems after the method of Schreinemakers geometric approach. U.S. Geological Survey Bulletin 1225.

Figure Captions

Figure 1. a: Diffraction image before integration, collected at 144 GPa and 3025 K. b: Diffraction pattern from part A integrated azimuthally. Peaks correspond to B2-NaCl, B1-FeO, and hcp-Fe. c: Diffraction pattern collected at 151 GPa and 1665 K, integrated azimuthally, with peaks corresponding to B2-NaCl, B8-FeO, and hcp-Fe.

Figure 2. Equation of state of B1-FeO. Filled circles: this study. Open triangles: Ozawa et al. (2010). Open squares: Seagle et al. (2008). Open diamonds: Campbell et al. (2009). All data and isotherms are color-coded by temperature range according to the legend. Isotherms are calculated using the parameters in Table 1 for the midpoint of the temperature range indicated, and they do not extend above the melting curve of Fischer and Campbell (2010).

Figure 3. Equation of state of B8-FeO. Filled circles: this study. Open triangles: Ozawa et al. (2010). \times : Kondo et al. (2004). Cross: Fei and Mao (1994). Errors in volume from this study were fixed at $\pm 0.1 \text{ cm}^3/\text{mol}$ when they could not be constrained by the data. Fei and Mao (1994) do not report an error in pressure. All data and isotherms are color-coded by temperature range, as in Figure 2. Isotherms are calculated using the parameters in Table 1 for the midpoint of the temperature range indicated, and they do not extend above the melting curve of Fischer and Campbell (2010).

Figure 4. High P - T phase diagram of wüstite. Pink symbols: stability field of B8 (NiAs-type) FeO. Blue symbols: stability field of B1 (NaCl-type) FeO. Filled circles: this study. \times : Kondo et al. (2004). Open triangles: Ozawa et al. (2010). Brown lines: phase boundaries of rhombally-distorted wüstite (Fei and Mao, 1994). Black line: melting curve from Fischer and Campbell (2010), extrapolated (dashed line) using Lindemann melting law. Gray: approximate geotherm, after Boehler (1996). This study and Ozawa et al. (2010) report phase stability of stoichiometric FeO, while Kondo et al (2004) used $\text{Fe}_{0.95}\text{O}$, Fei and Mao (1994) used $\text{Fe}_{0.98}\text{O}$, and Fischer and Campbell (2010) used $\text{Fe}_{0.94}\text{O}$.

Figure 5. Core density deficit. Grey line: PREM (Dziewonski and Anderson, 1981). Blue line: density profile for B1-FeO, calculated from the parameters listed in Table 1. Orange line: density profile for hcp-Fe, calculated from the equation of state of Dewaele et al. (2006). Solid lines follow an adiabatic temperature profile for a CMB temperature of 4000 K. Dashed lines indicate the effect of a ± 500 K uncertainty in the CMB temperature.

Figure 6. Fe–FeO oxygen fugacity buffers at high pressures and temperatures. The 1 bar buffer curve was calculated from Chase (1998), and high pressure curves were calculated from Eq. (2) using fits to the data like those in Figure 2. These buffers are only valid for B1-FeO in the high-spin state.

Table 1. Equation of state parameters for B1- and B8-FeO.

	B1-FeO	B8-FeO
V_0 (cm ³ /mol)	<i>12.256^a</i>	11.997 ± 0.018
K_0 (GPa)	149.4 ± 1.0	137.8 ± 0.9
K_0'	3.60 ± 0.04	<i>4</i>
θ_0 (K)	<i>417^b</i>	<i>417^b</i>
γ_0	1.41 ± 0.05	1.73 ± 0.12
q	<i>0.5</i>	<i>1</i>

Entries in italics were held fixed in the fit.

^aMcCammon and Liu (1984)

^bStixrude and Lithgow-Bertelloni (2007)

Supplementary Material

Supplementary Table S1. Pressure-volume-temperature data from synchrotron X-ray diffraction experiments. Pressures are determined from the unit cell volumes of hcp-Fe using the equation of state of Dewaele et al. (2006). Reported temperatures are corrected for an axial temperature gradient.

Supplementary Table S2. Tabulation of the Fe-FeO oxygen fugacity buffer at high pressures and temperatures.

Figure 1a

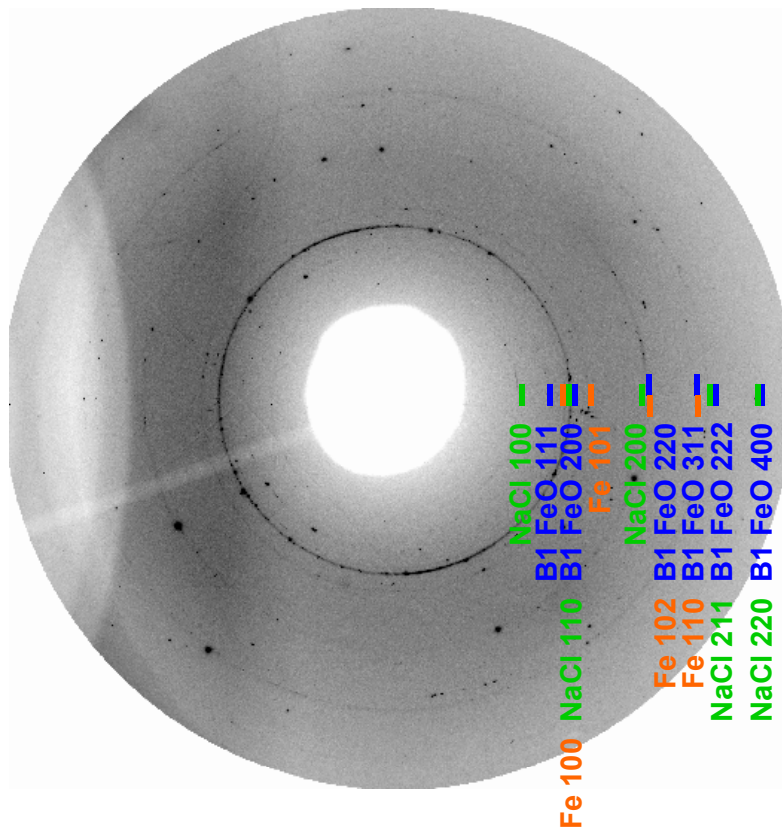


Figure 1b

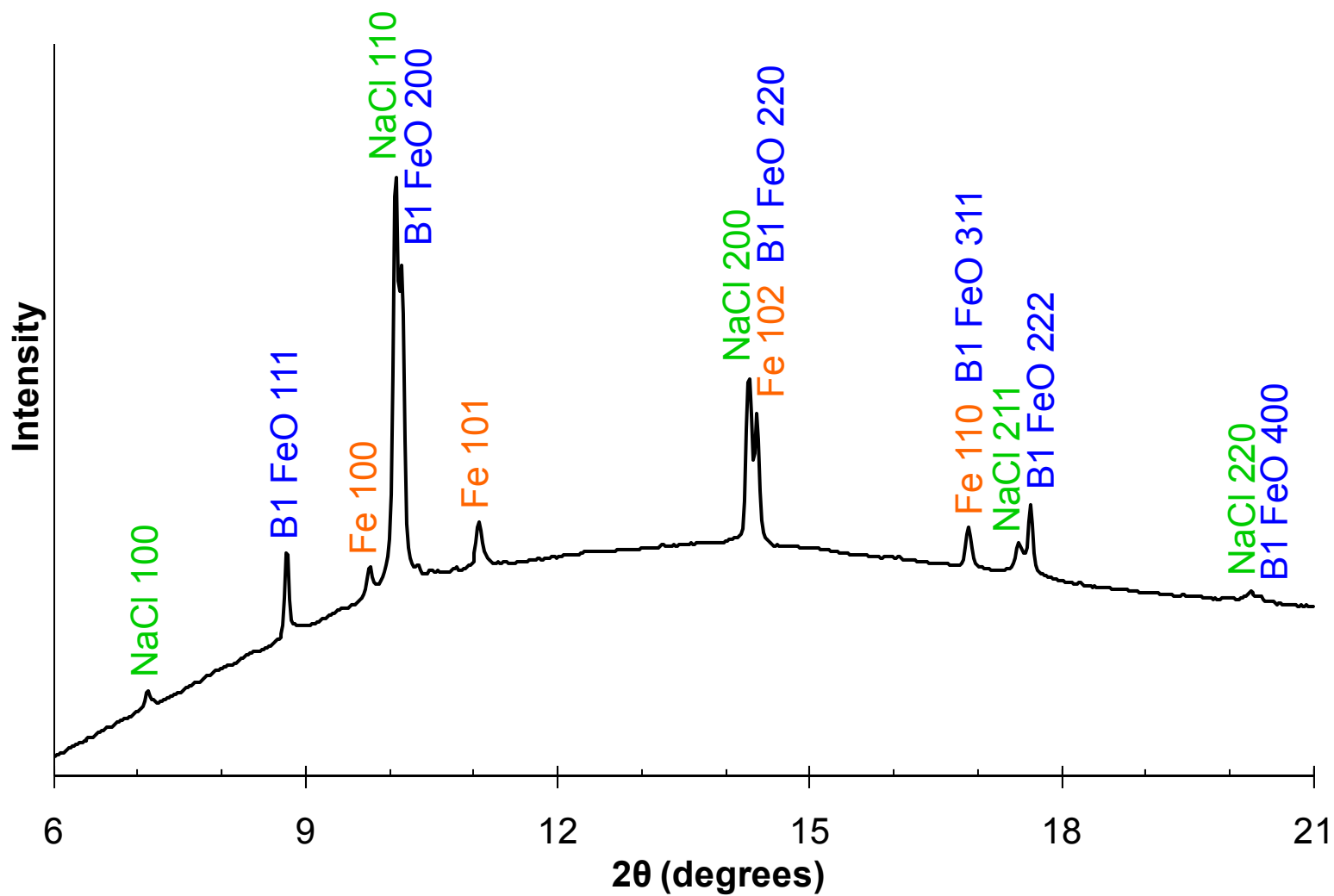


Figure 1c

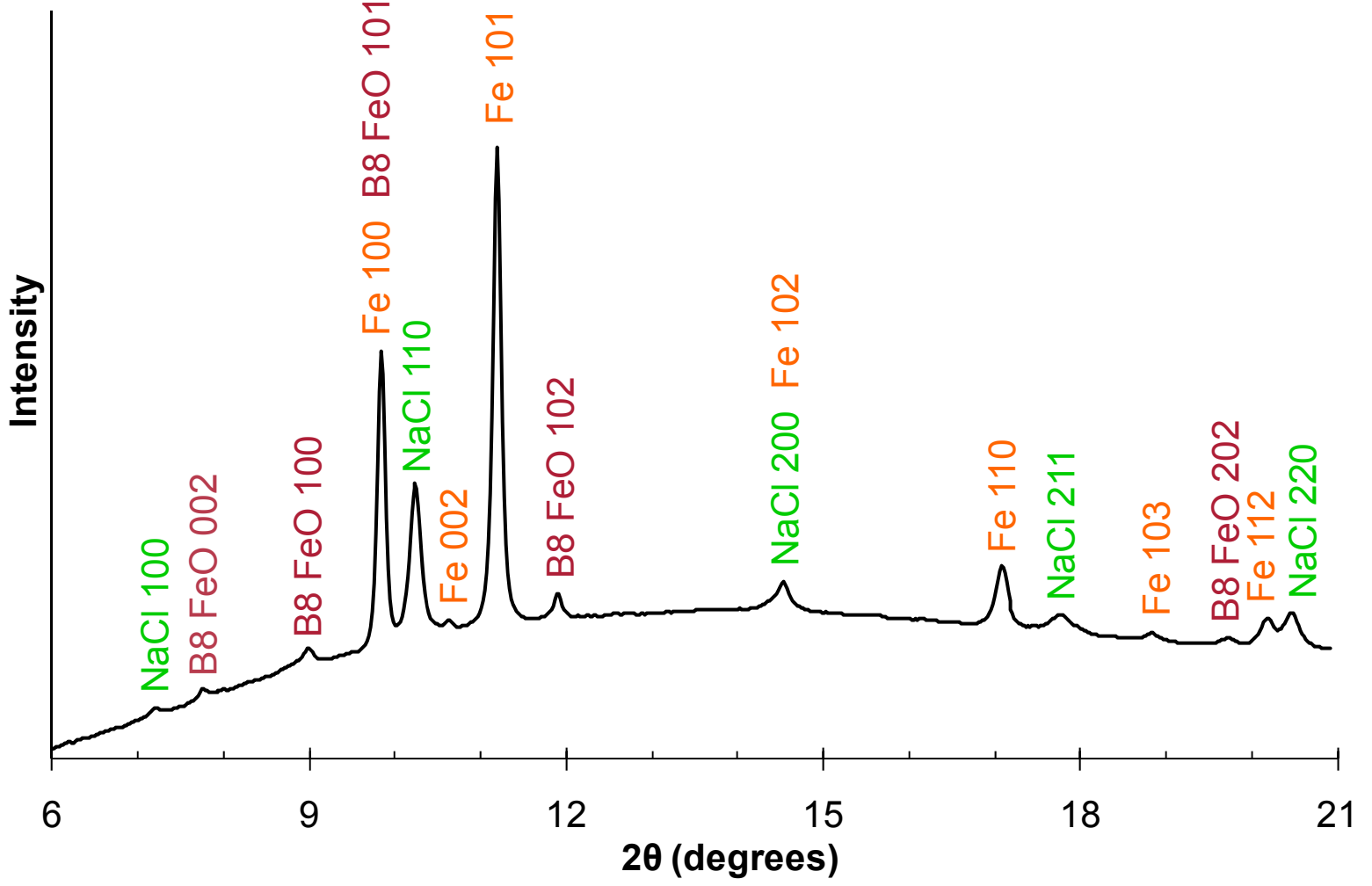


Figure 2

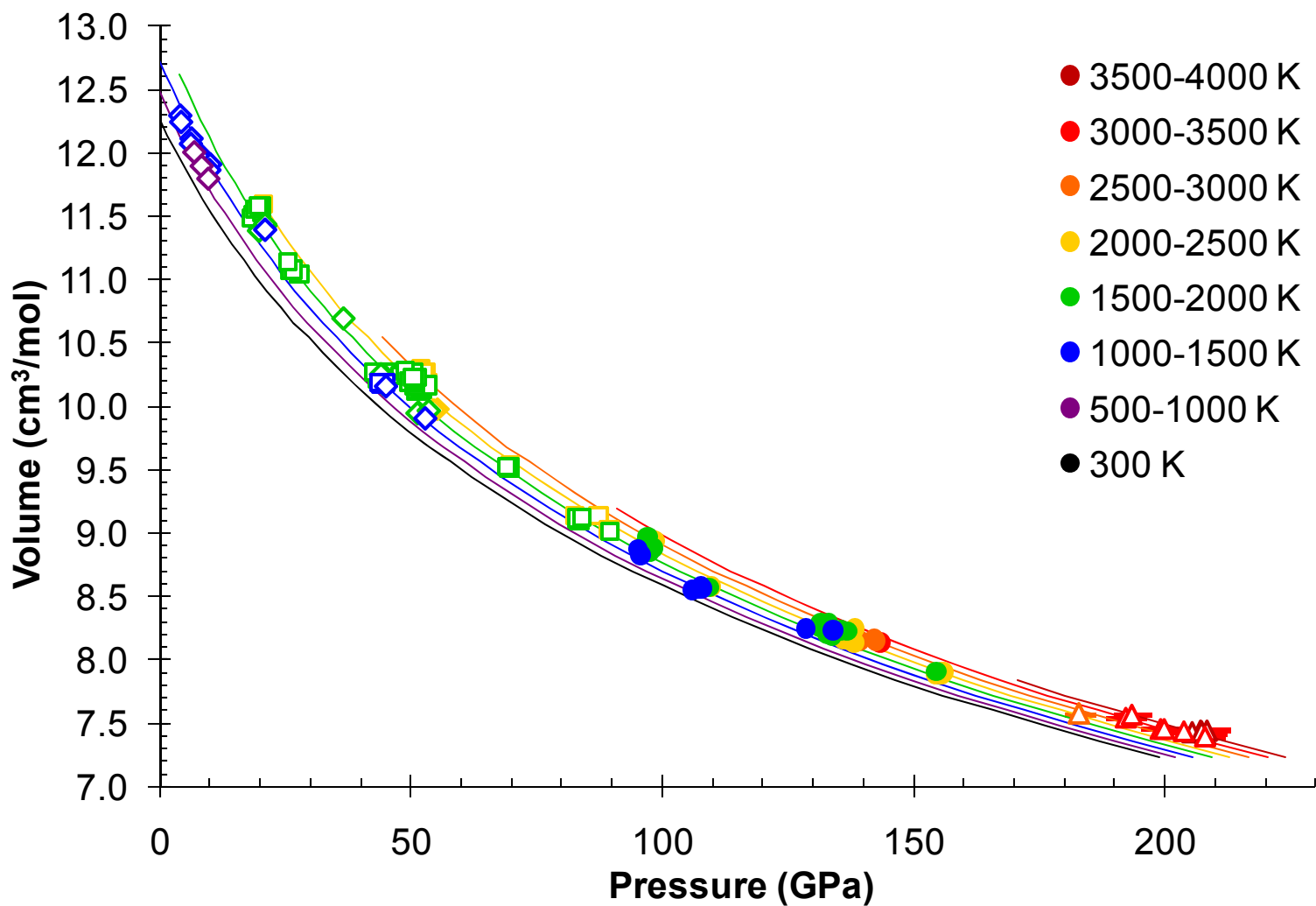


Figure 3

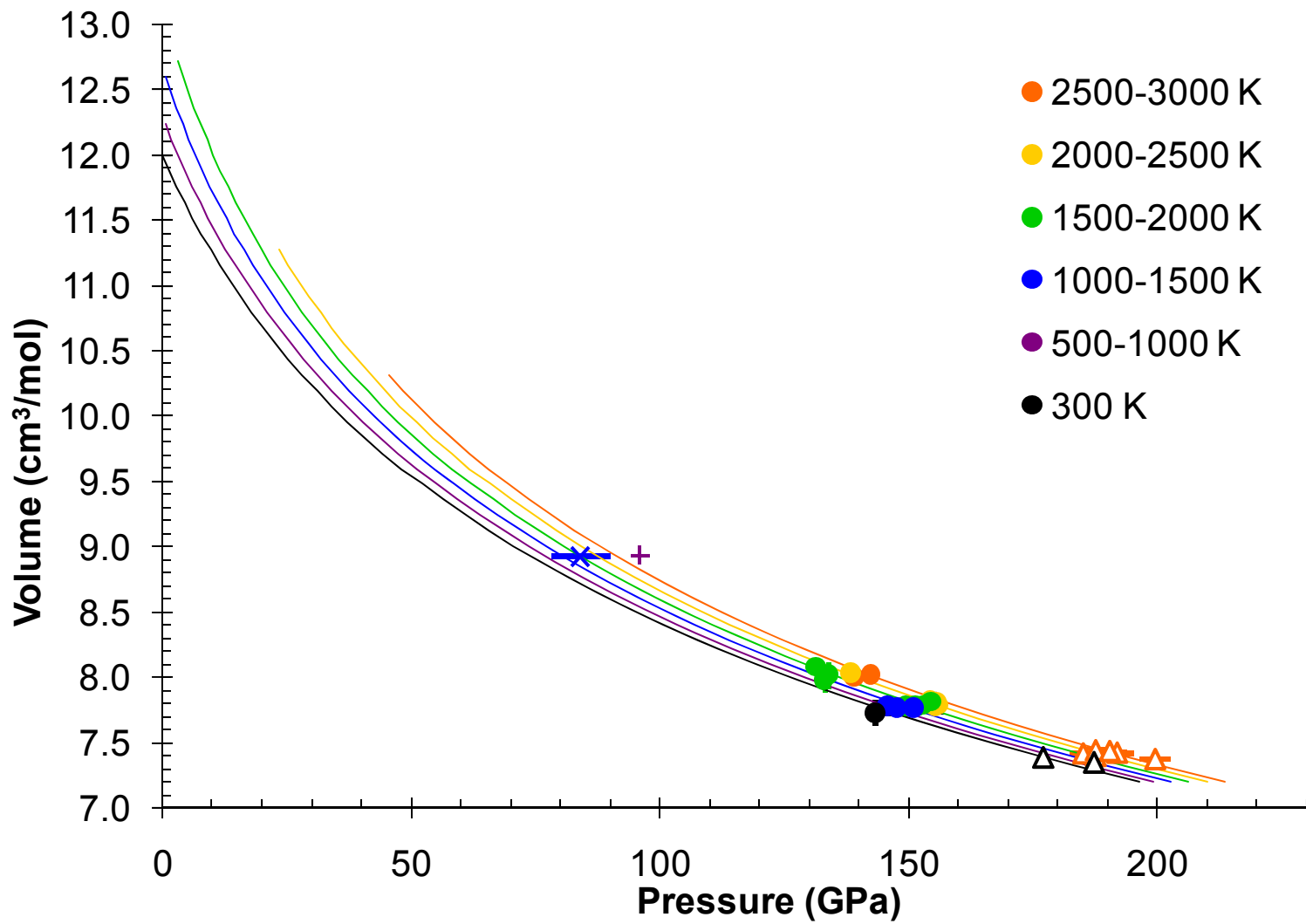


Figure 4

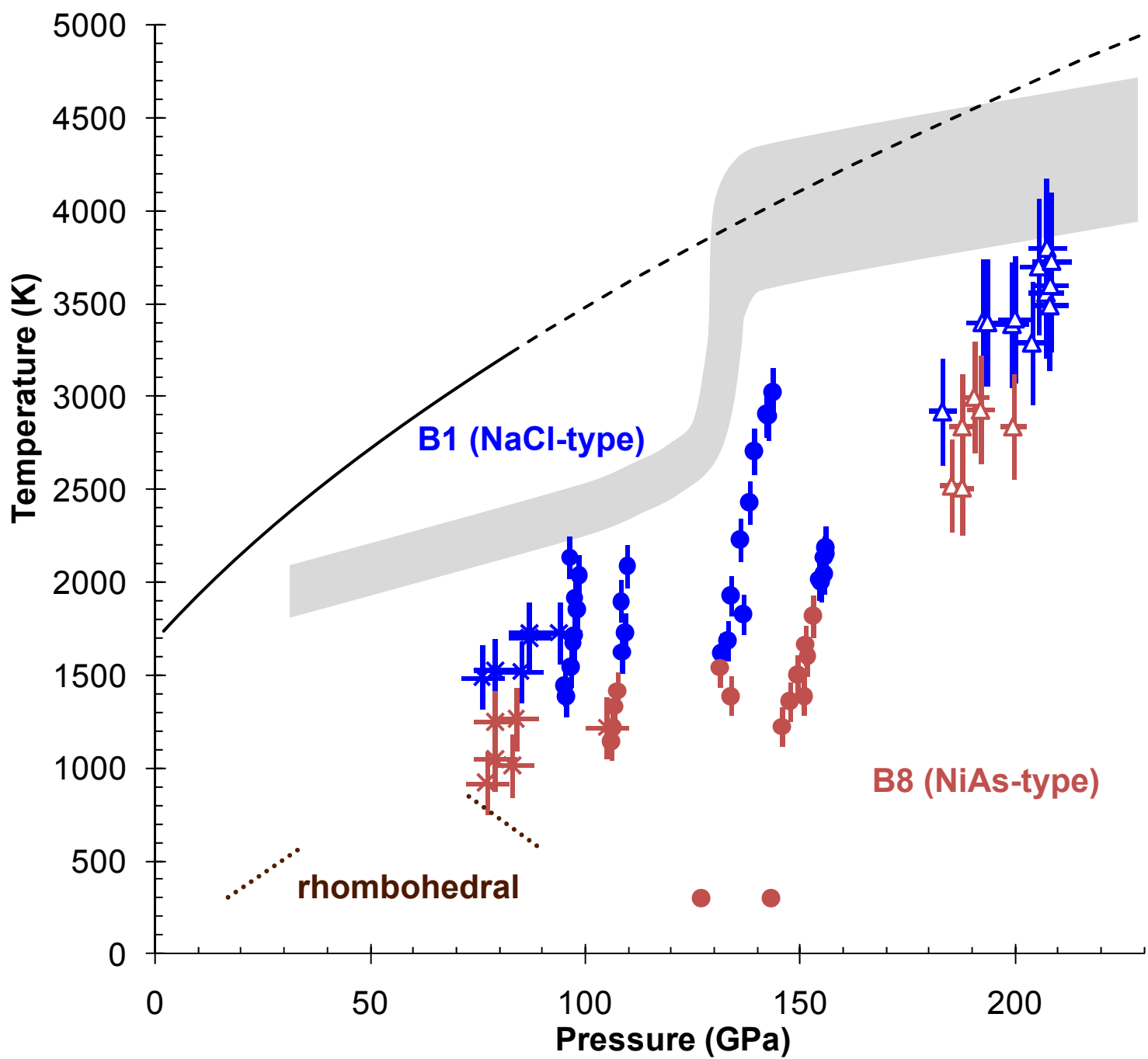


Figure 5

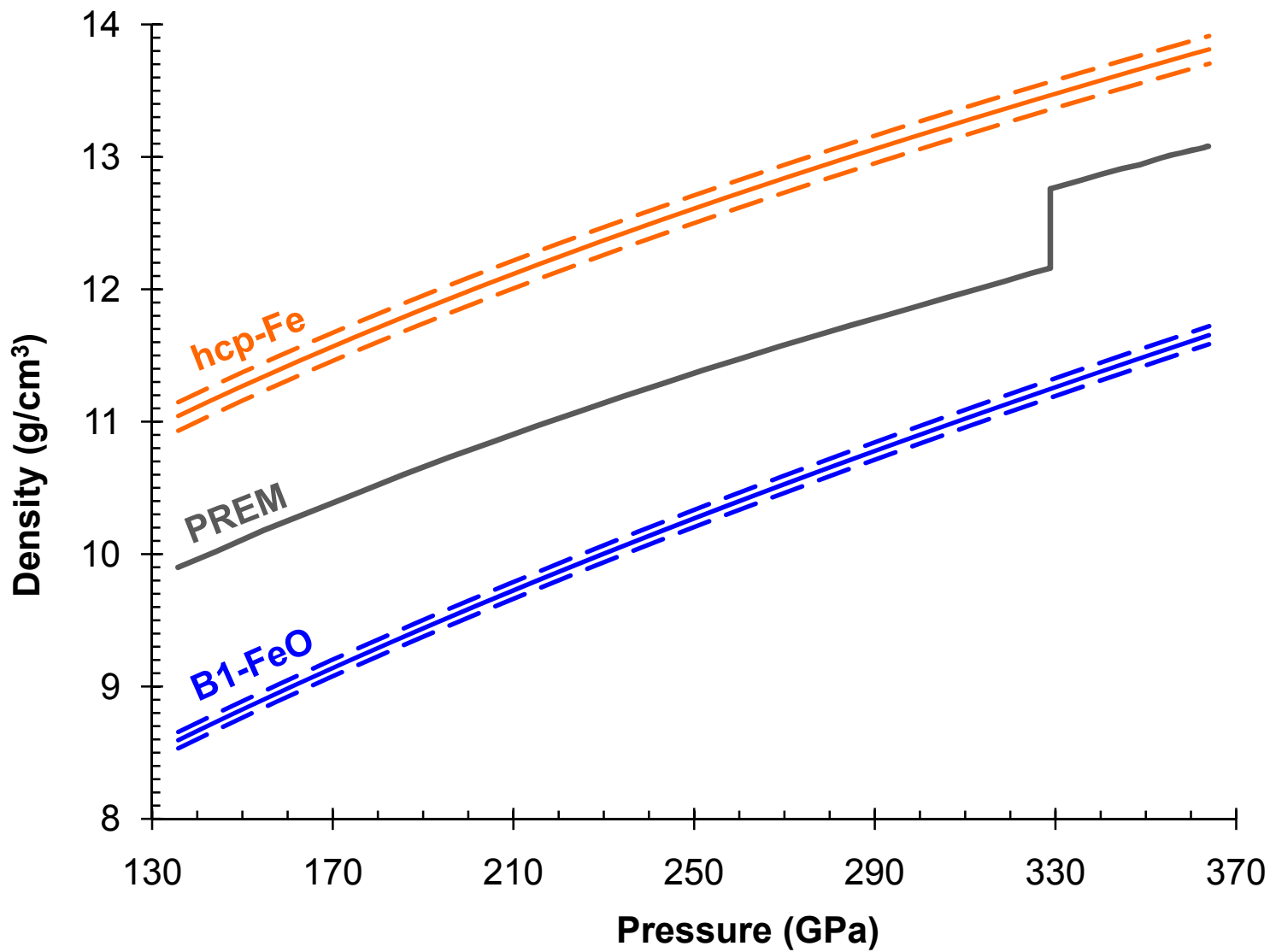


Figure 6

